UNIVERSITY OF READING

Department of Mathematics

Drag and Momentum Fluxes Produced by Mountain Waves

By

Yu Chau Lam

Supervisor: Dr. Miguel Teixeira

A dissertation submitted in partial ful llment of the requirements for the degree of MSc in Mathematical and Numerical Modeling of the Atmosphere and Oceans

October 2013

Declaration

I con rm that this is my own work, and the use of all material from other sources has been properly and fully acknowledged.

Signed .....

Yu Chau Lam

October 2013

Abstract

Acknowledgments

Contents

List of symbols

$= (k_1; k_2; k_3)$	3D total wave vector
$\mathbf{k} = (k_1; k_2; 0)$	Horizontal projection of (referred as horizontal wave)
k_{12}	The magnitude of k
$!$	Angular frequency
$\mathbf{v}_p = (v_{p1}; v_{p2}; v_{p3})$	3D phase velocity
$\mathbf{v}_g = (v_{g1}; v_{g2}; v_{g3})$	3D group velocity
$\mathbf{u} = (u; v; w)$	Full velocity of the wind
f	The Coriolis parameter
p	Pressure
	Potential temperature
	Density of air
T	Temperature
g	Magnitude of gravitational acceleration
R_d	Ideal gas constant for dry air
N	The Brunt-Vaisala frequency
	The Doppler-shifted intrinsic frequency
m	The vertical wave number
L	The inverse of m
$\hat{q}$	The Fourier transform of the quantity q, unless otherwise specified
h	The orography profile
h_m	The height scale of the orography
a	The width scale of the orography
$\hat{a}$	Non-dimensionalized width scale of the orography
	Vertical streamline displacement
l	The Scorer parameter
Ri	The Richardson number

Chapter 1

Introduction

A stably strati ed atmosphere has the important property of supporting the propagation of waves with di erent scales, from the large-scale planetary waves such as Rossby waves to the small-scale sound waves. Some of these waves play a crucial role in meteorological phenonema (e.g. Rossby waves), while others do not (e.g. sound waves). Nowadays, with the ever improving technology, numerical weather prediction plays an increasingly important role in weather forecast. However, no matter how advanced the modern meteorological models are, there are still many phenomena that they cannot capture, for example small-scale but important processes like convection, cloud microphysics, turbulence, etc. The subject of this study, terrain-generated gravity waves, are also one of these processes. These small-scale processes can only be captured by parametrization schemes, and therefore a deep understanding of them is necessary in order to develop good parametrizations.

As their name tells, terrain-generated gravity waves are wave phenomena generated by orography. One distinctive feature of terrain-generated gravity-waves is that they are stationary to observers on the ground (Lin (2007); Nappo (2012)). From the foregoing discussion we will learn that these waves are non-dispersive since all wave components have the same phase speed, which is 0. Terrain-generated gravity waves are worth studying since their presence acts to transport horizontal momentum of the mean ow vertically. As the waves propagate upward to a certain high level, they may break and generate turbulence, which is known as clear-air turbulence (CAT) (Nappo 2012). Studies have shown that such wave-breaking zones often coincide with critical levels (Grubi sic and Smolarkiewicz (1997); Shutts and Gadian (1999)). The detailed behavior of gravity waves in the vicinity of critical levels will be studied in chapter 2 and appendix A.

There are mainly two kinds of terrain-generated gravity waves, namely vertically-propagating mountain waves and trapped lee waves (Nappo 2012). One signi cant di erence between them is that trapped lee waves appear only on the downwind side of mountains. As will be discussed in later chapters, the atmosphere may sometimes be unable to support wave propagation for certain waves at some levels. As such waves propagate upward from the obstacle, wave re ection will occur and cause the waves to be trapped in the lower atmosphere and extend only horizontally (Nappo 2012). As a result, such waves usually have less impact on the high atmo-

sphere.

Di erent from trapped lee waves, vertically propagating mountain waves can extend both horizontally and vertically, and hence have a much greater impact on the high atmosphere, since transport of momentum and energy can reach much higher levels. In fact, mountain waves even play an important role in modulating the atmospheric global circulation (McFarlane (1987); Teixeira and Miranda (2004)).

1.1 Aims and Outline of this thesis

Orographically generated gravity waves in uence the atmosphere by exerting a drag force on it, which acts to decelerate the mean ow. At the same time, horizontal momentum associated with the mean ow is transported upward to the upper atmosphere. These processes are of small scale and common in the atmosphere. In order to produce accurate numerical weather predictions, such small-scale processes must be parametrized in large-scale meteorological models, due to the lack of su cient resolution to capture their details. Parametrizations of these processes have to be developed by rst studying their detailed dynamics in idealized settings and summarizing the variation of quantities that have an important impact on the atmosphere. The main aim of this dissertation is to study the variations of important quantities associated with the mountain waves, such as the surface drag and momentum uxes for ow over an idealized 3D isolated mountain, subject to di erent wind pro les, in both hydrostatic and non-hydrostatic conditions. Non-hydrostatic e ects associated with the wind pro le will be examined to see how they a ect the variation of those relevant quantities. This is practically important since the current parametrization schemes assume a hydrostatic atmosphere, which is certainly not always valid. Moreover, these wind pro les are designed speci cally for investigating the interactions between the gravity waves and critical levels, where the wave energy is known to be signi cantly absorbed and wave breaking may easily occur (Broad (1995); Shutts (1995)).

In this chapter, most of the basic concepts, which are necessary for the discussion in the later chapters, will be introduced. Those concepts include the group velocity and the dispersion relation of the gravity waves, as well as the linear theory, which uses the important Boussinesq approximation, and the derivation of the Taylor Goldstein equation. In fact, solving the Taylor-Goldstein equation subject to di erent types of ow is the main target of this study, since all the information required can be obtained from the solution to this equation.

In chapter 2, an example using a 2D mountain ridge and a constant wind pro le will be illustrated, which allows us to classify the di erent regimes of the solution space of the Taylor-Goldstein equation. The discussion in the later chapters will be based on this classi cation. Next, two important quantities will be introduced, namely the surface drag and the vertical momentum uxes. The discussion will rst explain the physical meaning of these quantities by looking at a 2D mountain ridge example, and then give their mathematical formulations.

Chapter 3 and 4 contain the main results of this study, which are divided into the hydrostatic

and non-hydrostatic limits. Di erent approaches have been used in each limit, such as deriving exact analytic solutions, use of the WKB approximation, and di erent numerical approaches.

can be calculated easily from the following relation

$$\frac{1}{\lambda}^2 = \frac{1}{\lambda_x}^2 + \frac{1}{\lambda_y}^2 + \frac{1}{\lambda_z}^2; \tag{1.4}$$

where λ_x, λ_y and λ_z are the wave lengths of waves projected onto the three coordinate axes.

For simplicity, let us now consider a 2D case in the x-z plane. Fixing a particular position $(x_0; z_0)$ at time $t = 0$, the phase of the wave associated with this point is $\phi_0 = kx_0 + mz_0$. The wave vector, lines of constant phase and total wave length are illustrated in gure (1.1(a)). As time t evolves, the lines with constant phase evolve continuously. The velocity of motion of these lines de nes the phase velocity, which is given by the total wave length divided by the period of oscillation, and its direction is along the wave vector,

$$v_p = \frac{\lambda}{T} = \frac{\omega}{k}. \tag{1.5}$$

The projections of the phase line velocities onto the two axes give the phase velocity v_{pi} along each axis i, and they are related to the total phase velocity via the following equation,

$$\frac{1}{v_p}^2 = \frac{1}{v_{px}}^2 + \frac{1}{v_{pz}}^2; \tag{1.6}$$

which in fact can be derived by using equation (1.4).

(a) (b)

Figure 1.1: (a) A schematic diagram showing a wave with wave vector . The red lines indicate lines of constant phase. Note that λ_x and λ_z are both longer than , and they satisfy the relation of equation (1.4). (b) A schematic diagram showing a cross-section of a ring-wave on water N small oscillations are superposed on at the surface of the ring-wave, each with a di erent phase speed $c(k_j)$, j = 1, 2, 3, ... , N. The velocity of the main ring-wave is given by u_g, which is in fact the group velocity of the wave. (Source: Nappo (2012))

1.2.2 The group velocity and the dispersion relation

In fact, the phase of a wave simply represents a pattern of the oscillation. So, the phase velocity refers to the movement of this pattern, but not to the movement of physical quantities. A more interesting problem would be to understand how fast waves transport energy and momentum. Indeed, wave energy and momentum must be carried with the group velocity of the wave, i.e. the velocity of motion of the wave packets.

Usually, oscillations occur as a result of overlapping of waves with a band of wave numbers (or wave vectors). In 1978, Lighthill observed that as a stone falls into a tank of water, a circular ring-wave is generated in the water, which expands in the radial direction and spreads outward (Nappo 2012). Moreover, as the circular ring-wave moves, small oscillatory phases are observed on its surface, which appear to move at a di erent velocity relative to the ring. The ring-wave, indeed, consists of waves with a continuous band of wave numbers, which have di erent phase speeds on the water surface and hence cause the observed relative motion. However, those small phases only appear on the surface of the ring-wave, but as they leave it, their amplitude becomes zero. If the phase of a wave really carried energy, then the small phases should be sustained without being destroyed. Therefore, the fact is that those small phases have no energy content, while the energy is carried by the ring-wave. In fact, the appearance of the moving ring-wave is due to the outward propagating energy, which allows the oscillations to appear and take the shape of a water ring. Therefore, the velocity of the moving wave packet is de ned to be the group velocity.

The mathematical formulation of the group velocity will just be presented here without derivation. In general, for a 3D case, the oscillation frequency$!$ can be expressed as a function of wave numbersk_i, $i = 1; 2; 3$. The group velocity $\mathbf{v}_g = (v_{gx}; v_{gy}; v_{gz})$ can be written as

$$v_{gx} = \frac{@!}{@k}$$

1.3 Linear Theory

The motions of the atmosphere under the assumption of inviscid adiabatic ow are governed by the complicated primitive equations set (1.8), which contains 5 non-linear di erential equations. Despite the fact that the primitive equations can capture many di erent phenomena of the atmosphere, they contain more formation than necessary, including unimportant wave phenomena such as sound waves, which do not have any meteorological signi cance. Such `noise' embedded in the initial condition would cause numerical instability in meteorological models (Lin 2007). Therefore, appropriate simpli cations to the primitive equations are necessary for studying the dynamics of the atmosphere. In this section, the result after those approximations will be stated, but the derivation will not be presented. Interested readers may consult any standard text books on atmospheric uid dynamics.

$$\frac{Du}{Dt} \quad fv = \quad -\frac{1}{}\frac{@p}{@x} \tag{1.8a}$$
$$\frac{Dv}{Dt} + fu = \quad 1$$

p can be written as

$$(x;y;z;t) = \quad _r(z) + \quad ^0(x;y;z;t); \tag{1.9a}$$

$$p(x;y;z;t) = p_r(z) + p^0(x;y;z;t) \tag{1.9b}$$

and that the magnitude of perturbations ^{0} and p^0 is much smaller than that of those reference states $_r$ and p_r. Then, in the subsequent simpli cations, we may neglect the e ect of ^{0} in all equations, except the vertical momentum equation (Booker and Bretherton 1967). This is because the atmosphere supports small-scale waves mainly via two mechanisms: one is the compression force, and another is the buoyancy force (Lin (2007); Nappo (2012)). The compression force arises from the compressibility of air, which produces acoustic waves with short wave length, such as sound waves. Such short waves are regarded as `noise' in the investigation of atmospheric dynamics. The buoyancy force is due to the contrast of density between an

is negligible, and then the nal result is

$$\frac{@u'}{@t} + U\frac{@u'}{@x} + V\frac{@u'}{@y} + w'\frac{@U}{@z} \qquad fv = \qquad \frac{@}{@x}\left(-\frac{p'}{r}\right) \tag{1.12a}$$

$$\frac{@v'}{@t} + U\frac{@v'}{@x} + V\frac{@v'}{@y} + w'\frac{@V}{@z} + fu = \qquad \frac{@}{@y}\left(-\frac{p'}{r}\right) \tag{1.12b}$$

$$\frac{@w'}{@t} + U\frac{@w'}{@x} + V\frac{@w'}{@y} = \qquad \frac{1}{r}\frac{@p'}{@z} + \frac{g}{T_0}T' \tag{1.12c}$$

Chapter 2

Flow over a 2-D isolated mountain

In this chapter, we are going to investigate mathematically the formulation of terrain generated gravity waves and some relevant physical quantities, by illustrating an example of a two-dimensional mountain ridge with a constant basic wind pro le. Terrain generated gravity waves a ect the atmospheric circulation by transporting energy and momentum of the mean ow from the lower atmosphere to the upper atmosphere and hence contribute to modify the global circulation (McFarlane 1987). Several important quantities, such as the surface drag, wave momentum ux, and the critical level will be formulated mathematically to facilitate the discussion in later chapters, which will extend the investigation to 3-dimensional space.

As will be shown in the 2-D example, the ow may exhibit di erent behaviors for di erent horizontal wave numbers k. In the case where the atmosphere is well strati ed and the mountain is broad and gentle, gravity waves can be supported by the buoyancy force and are capable to propagate vertically in the atmosphere. However, if the atmosphere is weakly strati ed, or with strong basic wind, gravity waves may not be able to propagate vertically and have to be decaying throughout the atmosphere (Nappo 2012). Such di erent types of ow can be classi ed into di erent regimes of the wave solution. The exploration of di erent solution regimes enable us to distinguish the criteria supporting the propagation of gravity waves.

2.1 Mountain pro le

In this section, we consider a bell-shaped mountain (or the so called Witch of Agnesi mountain pro le),

$$h(x) = \frac{h_m a^2}{x^2 + a^2} \tag{2.1}$$

where h_m is the mountain height and a is the horizontal scale of the mountain. This mountain form had been widely used in many published books and papers (Lin (2007); Nappo (2012) and

Teixeira and Miranda (2009)), because of the simple form of its Fourier transform,

$$\hat{h}(k) = \frac{h_m a}{2} e^{-|ka|}; \tag{2.2}$$

which will greatly facilitate the calculation of the wave solution. It turns out that the Fourier transform of the orography pro le plays an important role in the process of generating gravity waves (Lin 2007). By Fourier analysis, we know that a periodic function on a real axis takes a discrete wave spectrum, i.e. the constituent wave numbers are discrete. However, if the function is not periodic, such as an isolated mountain pro le in this case, the function is then composited of a continuous band of wave numbers k (Nappo 2012). Hence, the steady state Taylor-Goldstein equation has to be solved for each of these wave numbers in order to compute those relevant quantities, such as the pressure perturbation, surface drag and vertical momentum uxes, etc. Figure (2.1(a)(b)) shows the distribution of the bell-shaped mountain and the product of k and $\hat{h}(k)$. The importance of the function $k\hat{h}(k)$ will be discussed in the coming section.

(a) $h(x)$ (b) $k\hat{h}(k)$

Figure 2.1: (a) shows an isolated bell-shaped mountain located at the origin, with mountain height h_m equal 1 unit (or equivalently the scale is normalized by the height of the mountain), while its scale width is $a = 10\ h_m$. (b) shows the distribution of $k\hat{h}(k)$, which has its maximum at the wave number $1=a = 0:1$.

2.2 Di erent regimes of solution

In chapter 1, by taking the Fourier transform of equation (1.12), we have derived the Taylor-Goldstein equation. In this subsection, a detailed solving process of equation (1.14) for $\hat{w}(k)$, which is the Fourier transform of the vertical velocity perturbation w^0, will be presented. The procedure follows the idea in the book by Lin (2007).

Consider now the 2D steady-state form of the Taylor-Goldstein equation (1.14):

$$\hat{w}''(z) + (l(z)^2 - k^2)\hat{w}(z) = 0 \tag{2.3}$$

With the above equation, now it is an appropriate time to distinguish the di erent regimes of the solution $w'(z)$. From equation (2.8), given a particular value of k, the contribution of the corresponding wave component e^{ikx} is weighted by the factor $k\hat{h}(k)$, which is equation (2.2) multiplied by k. This implies that the total budget of a particular horizontal wave number k is governed by the Fourier transform of the orography pro le. Thus, if most of the k contributed from the orography is bigger than l, then the second integral in equation (2.8) dominates. This is referred to as the irrotational (potential) ow limit. Conversely, if the k contributed from the orography is mostly smaller than l, then the rst integral in equation (2.8) dominates: this is the hydrostatic ow limit. Figure (2.1(b)) shows the distribution of $k\hat{h}(k)$ as a function of k, which has a maximum value of $h_m=(2e)$ at $k = 1=a$ and decays exponentially afterwards. Thus, the value of $1=a$ de nes the scale of the horizontal wave number. Therefore, a condition for the ow to be hydrostatic is

$$\frac{1}{a} \quad l \quad \frac{N}{jUj} \qquad \text{or equivalently,} \quad \frac{Na}{jUj} \quad 1 \tag{2.9}$$

And we de ne the non-dimensional constant $\hat{a} = Na=jUj$. Therefore, the hydrostatic assumption is generally valid if $\hat{a}$ 1 (Teixeira et al. (2004); Teixeira and Miranda (2004)).

It turns out in these two limits the vertical streamline displacement of the ow $(x;z)$ can be integrated exactly. First, we investigate the behavior of the ow when it is in the irrotational ow regime by assuming l k. In this limit, we can assume the rst integral can be neglected and $l = 0$.

$$\begin{aligned} w'(x;z) \quad & 2\mathrm{Re}\ U \int_0^{Z_1} ik\hat{h}(k)e^{\ kz}e^{ikx}dk \\ & = (\ h_m a)\,\mathrm{Re}\ U \int_0^{Z_1} ike^{\ kz}e^{ikx}e^{\ ka}dk \end{aligned} \tag{2.10}$$

The vertical streamline displacement $(x;z)$ is de ned by the equation $w' = U\frac{@}{@x}$ (Lin (2007); Nappo (2012)). The corresponding Fourier transform gives

$$\hat{}(k;z) = \frac{\hat{w}(k;z)}{ikU} \tag{2.11}$$

By using the above relation, $(x;z)$ can be calculated as (Lin (2007); Nappo (2012))

$$(x;z) = h_m a\mathrm{Re} \int_0^{Z_1} e^{\ k(z+a\ ix)}dk \quad = \quad \textit{Tf 14.697 15.382 Td [( )]TJ 5.758 -0.53}$$

equation (2.8) can be neglected. Thus $w^0(x;z)$ and $(x;z)$ can be integrated as

$$w^0(x;z) \quad 2\mathrm{Re}\ U \int_0^{\infty} ik \ \frac{h_m a}{2} \ e^{\ ka} e^{ilz} e^{ikx} dk \tag{2.13}$$

$$(x;z) \quad h_m a \mathrm{Re} \int_0^{\infty} e^{ilz} e^{\ k(a\ \ ix)} dk \ = \ \frac{h_m a \cos lz \quad x \sin lz}{x^2 + (z+a)^2}: \tag{2.14}$$

Figure(2.2) shows the ow trajectories and pressure perturbation under di erent regimes.

2.3 The surface drag and momentum uxes: conceptually

Figure 2.2 shows the streamlines $(x;z)$ and the pressure perturbation $p^0(x;z)$ in the di erent ow regimes described in the previous section. As shown in gure (2.2(a)), a important di erence between the irrotational ow and the other two types of ow is that the pressure distribution of irrotational ow is symmetric on both upstream and downstream sides of the mountain, while the pressure distribution is mostly asymmetric in the hydrostatic limit. It turns out that this asymmetric distribution of pressure plays a crucial role in the generation of the surface drag force and wave momentum uxes.

The formation of the drag force can be understood by using some basic mechanics (Teixeira et al. (2004); Teixeira and Miranda (2004); Nappo (2012)). The uneven distribution of pressure on two sides of the mountain contributes to a pressure-gradient force exerted to the obstacle by the ow (Lin (2007); Teixeira et al. (2004)). Then the famous Newton's third law of motion states that,

> For any force exerted by an object A on an object B, there is a reaction force exerted by object B on object A at the same time, with the same magnitude but opposite direction.

Therefore, the existence of a surface pressure gradient force on the mountain means that there is a reaction drag force exerted on the ow by the mountain. This drag force creates ow perturbation patterns which carry mean ow horizontal momentum and propagate upwards (Nappo 2012). The stronger the drag force the ow experiences, the greater the upward propagating momentum ux is. As a result, the drag force represents the total amount of horizontal momentum being able to be transported vertically to the upper atmosphere in the form of gravity waves (Teixeira and Miranda 2009). As we can see from gure(2.2(a)), gravity waves do not appear (the ow amplitude decays exponentially with height) in the case of irrotational potential ow due to the absence of the pressure di erence on the two sides of the mountain (and hence the drag force). For the other two types of ow, wavy patterns of the streamlines and pressure can be clearly observed in the vertical direction. Associated with them are strong surface pressure gradients and surface drag forces, which are consistent with the above analysis. These can be veri ed easily in gure 2.2(b) and 2.2(c).

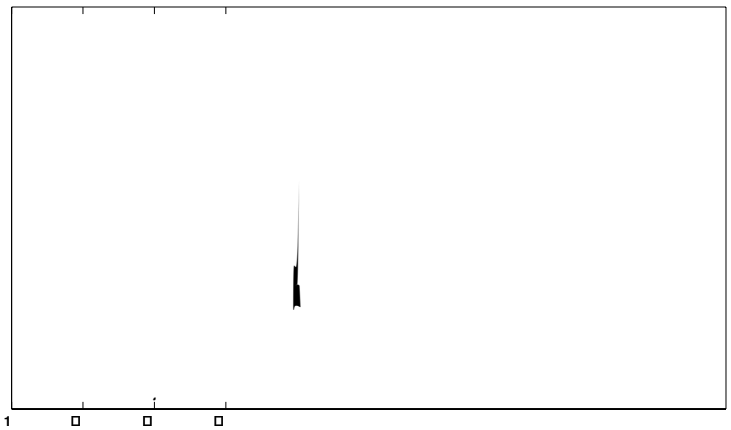

(a) Irrotational flow: $a = h_m = 1\text{km}$, $N = 0.01$, $U = 100\text{ms}^{-1}$

(b) Intermediate: $a = h_m = 1\text{km}$, $N = 0.01$, $U = 10\text{ms}^{-1}$

(c) Hydrostatic flow: $a = 10\text{km}$, $h_m = 1\text{km}$, $N = 0.01$, $U = 10\text{ms}^{-1}$

Figure 2.2: (a) shows a contour plot of the pressure perturbation (colored lines), and trajectories of the flow (black lines) in the irrotational potential flow. The flow is evanescent above the mountain. (b)(c) show filled contour plots of the pressure perturbation and trajectories of the

Mathematically, since the quantity l is actually the total wave number, while k is the horizontal wave number, the assumption that $l \quad k$ implies immediately that the total wave vector is almost vertically orientated. Moreover, the stationary nature of the mountain wave can be explained by the fact that the existence of a drag force arises from the surface orography, so the gravity wave patterns have to remain attached to the orography (which is their source).

2.4 The surface drag and momentum uxes: mathematically

With the conceptual discussion of the surface drag and momentum uxes in the previous section, in this section the mathematical formulation of these quantities will be illustrated. The approach follows books by Lin (2007) and Nappo (2012).

Recall that the surface drag D is created due to the net pressure gradient force resulting from the asymmetric pressure distribution on the orographic pro le. One equation directly related with the pressure gradient force is the horizontal momentum equation, i.e. the 2D version of equation (1.12a)

$$U\frac{@u}{@x} + w'\frac{@U}{@z} + \frac{1}{r}\frac{@p'}{@x}$$

In the above equation (2.20), the R.H.S is the integral of the product of the pressure and the elevation gradient, which is the net pressure gradient force experienced by the orography; while the L.H.S is the integral of the product of the horizontal momentum and vertical velocity, which is the stress force experienced by the mean ow. Therefore, we can see that equation(2.20) is in fact a statement of Newton's third law, as explained in the previous section.

Thus, the formal surface drag force (at $z = 0$) is de ned as

$$D = \int_{-1}^{1} \rho u' w' dx = \int_{-1}^{1} p' \frac{dh}{dx} dx; \tag{2.21}$$

which is actually equation (2.20).

Equation (2.20) de nes the surface drag in terms of the pressure gradient force at the surface. Despite the fact that the R.H.S loses its meaning above the surface, the quantity on the left hand side the L.H.S does not. However, this limitation can be avoided by replacing h by η, i.e. the vertical streamline displacement of the ow. Moreover, the product of $\rho u'$ and w' has the physical meaning of vertical advection of horizontal momentum. Thus, integrating this quantity over the entire real axis at any level describes the momentum ux at that level. Thus the momentum ux can be formulated as

$$M = \int_{-1}^{1} \rho u' w' dx \tag{2.22}$$

From this de nition we can see immediately that the momentum ux at the surface gives exactly the surface drag. In other words, this again demonstrates that the drag force gives the total amount the horizontal momentum ux that can be produced by the ow over the orography (Teixeira and Miranda 2009).

2.5 Height dependent Scorer Parameter

In the previous sections, we only focused on the situation when both the basic wind pro le $U(z)$ and the Brunt-Väisälä frequency N are constant with respect to height, i.e. a constant Scorer parameter. However, reality is not always that simple. The basic wind pro le can be easily altered by a lot of factors, such as variations of the surface temperature, or orographic distribution. In this situation, the Taylor-Goldstein equation (2.3) cannot be solved analytically in general for arbitrary wind pro les. Hence, numerical calculations are necessary for investigating the behavior of the atmospheric motions (Grisogono (1994); Shutts (1995); Shutts and Gadian (1999)).

Despite this di culty, the behavior can still be analyzed using reasonable simpli cations and assumptions. A common approach is to assume that the variations of the Scorer parameter (2.4) in the vertical direction are slow. Recall that when the Scorer parameter l is constant with

height, equation (2.3) admits wave solutions (2.7), in which the wave number is $m = \frac{p}{l}$

2-D and 3-D cases. In a 2-D situation, a critical level appears only when the basic wind $U(z)$ is zero at some height z_c, while in the 3-D case, it refers to the levels where the vector $\mathbf{U}$ is perpendicular to the horizontal wave vector number $\mathbf{k}$. In fact, the de nition of a critical level in the 3-D case is more general, in the sense that the 2-D de nition can be viewed as a restriction by reduction of dimensions. Following this point of view, it should be noted that the critical level in a 2-D situation is k-independent since the horizontal dimension contains only the x direction, so the dot product $\mathbf{U} \cdot \mathbf{k}$ can be zero if and only if $U(z) = 0$. But in a 3D situation, the critical level z_c is k-dependent, except when $\mathbf{U}(z) = 0$. Thus, Broad (1995) designates the critical level z_c at which $\mathbf{U}(z) = 0$ as a `total critical levels' in the 3-D situation. Moreover, with 3D orography, at any height z, there is always some wave vector $\mathbf{k}$ perpendicular to the basic wind $U(z)$. This means that every level in the atmosphere is the critical level for a certain wave vector $\mathbf{k}$. So this contributes to the so-called `critical layer', as opposed to discrete critical levels. Moreover, the k-dependent property of the critical levels contributes to a directional ltering e ect of critical layers (Broad (1995); Shutts (1995)). In chapter 3, a more detailed discussion about the e ect of critical levels in a 3-D situation will be presented.

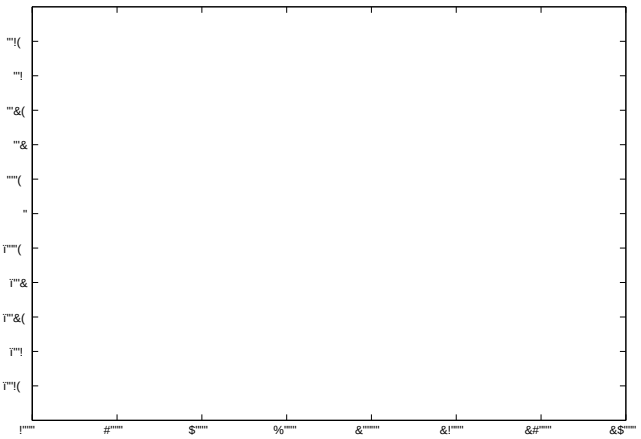

Figure 2.3: shows the behavior of the real (blue) and imaginary (green) parts of $w(z)$ around a critical level z_c for a particular wave vector $\mathbf{k}$ in a 3D situation. The wave becomes highly oscillatory as it approaches z_c (in fact its frequency approaches in nity), and the amplitude of the wave shows a shape drop (by a factor of $e^{\quad}$, with $\quad = 1{:}4234$ and $Ri = 2{:}276$ in this gure) once it passes through z_c. Both the units for the x and y-axis in this gure are arbitrary.

Chapter 3

Flow Over a 3-D Isolated Mountain in the Hydrostatic Regime

In this chapter, we are going to investigate mountain waves generated by flow over a 3-D isolated mountain in the hydrostatic limit. Two simple height-dependent wind profiles will be examined: a linear wind profile with directional shear and a turning wind profile. Reasons for choosing these wind profiles are that, first, they are simple and can be described easily by elementary functions, and second, the directionality of the wind profile allows the existence of a critical layer, i.e. a layer of the atmosphere in which any level is a critical level for a certain wave vector $\mathbf{k}$. Two methods, namely the WKB approximation and a numerical method developed by Siversten (1972), will be adopted to solve the Taylor-Goldstein equation, and their results will be presented and compared.

3.1 Setting of the problem

An inviscid, irrotational, steady flow can be captured by the steady-state version of the linearized 3-D Boussinesq equations (1.12), which can be used to derive the steady-state Taylor-Goldstein equation,

$$\hat{w}''(z) + \frac{N^2 k_{12}^2}{(Uk_1 + Vk_2)^2} \quad U$$

If the static stability coe cient N is real and varies gently with height as well as $\mathbf{U}$, then the consequence of this assumption is that any wave being considered can freely propagate vertically in the atmosphere, i.e. the associated solution of $w(z)$ must be in the form of a propagating wave at any level of the atmosphere. Therefore, wave re ection phenomenon does not occur. With this observation, it is possible to include only waves with upward propagating energy. The full atmospheric setting will be discussed next together with consideration of the critical layer and the wind pro le.

3.1.1 The critical layer

For ow over a 3-D isolated mountain, given a certain wave vector, the associated critical level is de ned as the altitude where the basic ow $\mathbf{U}$ is perpendicular to the horizontal wave vector $\mathbf{k}$. The e ect of the critical level is that the wave energy and momentum is e ectively attenuated and absorbed by a factor of e into the mean wind without being re ected (Grubi sic and Smolarkiewicz 1997), as discussed in chapter 2. Therefore, if the direction of the basic wind pro le turns with height, then it induces a continuous region in the atmosphere, in which each level is a critical level for a certain horizontal wave vector $\mathbf{k}$ (Shutts 1998). This region is the critical layer, as explained in chapter 2. Thus, the existence of a directional shear will be a necessary condition for the occurrence of such a layer. The e ect of such a layer is well summarized in the paper by Broad (1995), where it is shown

$$\mathbf{U}(z) \quad \frac{d \quad (z)}{dz} = 0; \tag{3.4}$$

where $(z) = (\ _x(z); \ _y(z); 0)$ is the wave stress vector, which is a generalized 3D version of the wave stress de ned inside the integral of equation (2.22).

Equation (3.4) states that the vertical gradient of the wave stress vector (and hence that of the vertical momentum ux vector) must be perpendicular to the mean wind $\mathbf{U}(z)$. This means that there is a ltering e ect of vertical momentum ux occurring along the direction perpendicular to the mean wind, which is the so-called `directional ltering e ect' of the critical layer. Such a ltering e ect throughout the critical layer is the interaction between the gravity waves and the mean wind (i.e. the deposition of wave energy and momentum) (Miranda and James (1992); Hines (1988); Shutts (1998)). For simplicity, we will only consider the situation where each horizontal wave vector $\mathbf{k}$ can have at most one critical level in the atmosphere, which means that the turning angle of the mean wind cannot exceed 180.

3.1.2 The wind pro les

As mentioned previously, two wind pro les will be examined in this chapter. The rst one is a linear wind pro le with directional shear, which can be formulated as

$$\mathbf{U}_{linear}(z) = (U(z); V(z)) = (U_0 \quad z; U_0); \tag{3.5}$$

where is the shear strength and U_0 is the surface wind magnitude for each component. Since $\mathbf{U}_{linear}(0)$ at the surface has both x and y components equal to U_0, this basic wind makes an

angle of =4 relative to the x-axis at the surface, and this angle approaches at in nity. But due to computational limitations, the domain being considered must be nite, and hence the wind can only turn by a certain angle $_{max}$ at the top of the domain z_{max}, as shown in g-ure (3.1(a)). Nevertheless, regardless of computational limitations, the atmosphere can still be considered as an in nitely extended troposphere with a height-independent stability constant N.

The second wind pro le being considered is the turning wind pro le,

$$\mathbf{U}_{turning}(z) = (U(z); V(z)) = (U_0 \cos(z); U_0 \sin(z)); \tag{3.6}$$

where is the rate of turning of the basic wind with respect to height and U_0 is the wind magnitude. As required, the wind can at most turn by an angle of from 0 at the surface to at the top of the computational domain z_{max}, as shown in gure (3.1(b)).

(a) Linear wind pro le (b) Turning wind pro le

Figure 3.1: (a) shows a schematic diagram of the linear wind pro le. (b) shows a schematic diagram of the turning wind pro le.

3.1.3 The mountain pro le

Similar to the case of a 2-D isolated mountain, the mountain being considered in this chapter is a 3-D circular bell-shaped mountain (i.eWitch of Agnesi mountain pro le),

$$h(x; y) = \frac{h_m}{(1 + (x=a)^2 + (y=a)^2)^{3=2}} \tag{3.7}$$

where h_m

The corresponding vertical wave number m can be calculated as

$$m = i\frac{w'}{w}$$
$$= (sgn)\ \frac{1}{z - \frac{U_0(k_1+k_2)}{k_1}}\ \ \frac{i}{2}\frac{1}{z - \frac{U_0(k_1+k_2)}{k_1}}: \qquad (3.12)$$

In fact, given a horizontal wave vector $k = (k_1; k_2)$, the associated critical level for this linear

The lower boundary condition is implicitly included in the solution form (3.14), so the boundary condition for (3.15) must be consistent with the upper radiation boundary condition.

Boundary condition

In fact, the correct boundary condition for (3.15) depends on the existence of the critical level. Fixing a particular wave number k, if a critical level does not exist, or it exists far away from the calculation domain, then we may assume that m reaches a constant at the top of the calculation domain, and the curvature of U is basically 0, so that $m'' = 0$ and the curvature term of (3.15) can be dropped. Thus,

$$m(z_{max}) = \frac{N k_{12}}{U(z_{max})k_1 + V(z_{max})k_2} \tag{3.16}$$

On the other hand, if a critical level appears within the domain or near the top of the domain, then the asymptotic behavior of m must be used. From appendix A, we know that $w\hat{}$ becomes highly oscillatory as z approaches z_c, which means that $m \to 1$ as $z \to z_c$. However, in nity is not a numerically favorable quantity, so a good way to tackle t3.11h316(no5(c)2-31m6(t3.1316(no5(316(ta

Error analysis

Since this numerical method solves for the vertical wave number m, instead of w, the error analysis will be based on the error associated with m. A wave vector k with its critical level z_c located near the surface is chosen. The integration of m

Generally speaking, the WKB method is an asymptotic series expansion for solving linear differential equations with spatially-dependent coefficients, e.g. a height-dependent Scorer parameter $l(z)$. This method is widely used in many different areas, such as wave mechanics, quantum

by de ning $Z = \varepsilon z$ and so $d/dz = \varepsilon d/dZ$ (Teixeira et al. 2004), which then yields

$$\varepsilon^2 \ddot{w} + \left[\frac{N^2 k_{12}^2}{(U k_1 + V k_2)^2} - \varepsilon^2 \frac{\omega^2 (U k_1 + V k_2)}{U k_1 + V k_2} \right] w = 0; \tag{3.23}$$

where d/dZ is denoted by a dot over the variable. Assume the solution of $w(z)$ takes the form of equation (3.22)

$$w(Z) = w(0) \exp\left(\frac{1}{\varepsilon} \sum_{j=0}^{\infty} i^j \int_0^Z m_j(\zeta) d\zeta \right); \tag{3.24}$$

where the point of reference is taken to be at the surface $z = 0$, so that the lower boundary condition can be naturally included. Substitute equation (3.24) into equation (3.23) and group terms of different powers of ε and ε. As both $\varepsilon, \varepsilon \to 0$, the dominant behavior is

$$\frac{\varepsilon^2}{2} m_0^2(z) + \frac{N^2 k_{12}^2}{(U k_1 + V k_2)^2} = 0. \tag{3.25}$$

We assume that the term $\frac{N^2 k_{12}^2}{(U k_1 + V k_2)^2}$ is large compared with ε and ε within the calculation domain. Then equation (3.25) is valid if and only if ε and ε are of the same order. Thus, we may set $\varepsilon = \varepsilon$, which then yields

$$m_0 = \frac{N k_{12}}{U k_1 + V k_2}. \tag{3.26}$$

This is the 0th-order WKB approximation. By comparing higher powers of ε, a set of equations for higher-order corrections can be obtained. First and second-order corrections (Teixeira and

propagating energy. Therefore, the desired branch m_i is chosen as

$$m_0 = \frac{Nk_{12}}{Uk_1 + Vk_2} \tag{3.29a}$$

$$m_1 = \frac{1}{2} i \frac{U_{-}k_1 + V_{-}k_2}{Uk_1 + Vk_2} \tag{3.29b}$$

$$m_2 = \frac{1}{8} \frac{Uk_1 + Vk_2}{Nk_{12}} \left(2 \frac{U_{\bullet}k_1 + V_{\bullet}k_2}{Uk_1 + Vk_2} + \left(\frac{U_{-}k_1 + V_{-}k_2}{Uk_1 + Vk_2} \right)^2 \right); \tag{3.29c}$$

which is consistent with the result of papers by Teixeira et al. (2004), Teixeira and Miranda (2009). Thus the WKB solution for $\hat{w}(Z)$ valid up to 2-nd order is

$$\hat{w}(Z) = \hat{w}(0) \exp \left[\frac{i}{\varepsilon} \int_0^Z \left(m_0(\zeta) + \varepsilon m_1(\zeta) + \varepsilon^2 m_2 \right) \right.$$

where is assumed to be arbitrarily small, so the dominant behavior of m_0 has been used in the second last equality ($G(\ ) \quad G'(z_c)\ e^{i}$ for on C_2). It turns out that this integral over C_2 is independent of the radius . Similarly, if $G'(z_c) < 0$, the contour goes above the singularity (i.e. the red curve must be used), and hence the integral value becomes $\frac{Nk_{12}}{G'(z_c)}$. Therefore, we can conclude that as z goes across z_c

$$\mathrm{Im}(I_0) = \frac{Nk_{12}}{|G'(z_c)|} = Ri^{-0.5}; \tag{3.39}$$

where Ri (de ned in appendix A) has the same scale as the Richardson number Ri.
Besides, expanding the exact factor obtained in appendix A using the Binomial theorem yields

$$= \sqrt{Ri \quad 0.25} = Ri^{0.5} \quad \frac{1}{8Ri^{0.5}} + \ldots \tag{3.40}$$

Thus the contribution of m_2 in the contour integral will give the factor $\frac{}{8Ri^{0.5}}$ (see the paper by Teixeira and Miranda (2009)), which is the same as the second term in (3.40). In fact, higher-order corrections to the amplitude factor can be obtained by the even-order terms of m_i, i.e. $m_0; m_2; m_4; \ldots$. Moreover, (3.40) implies that a nite truncation will be a good approximation if $Ri \quad 1/8$ (see the paper by Whitten and Riegel (1973)). In general, we are only interested in $Ri > 1/4$, since otherwise there would be dynamical instability and the mountain waves would break down. Therefore, the above analysis shows that the WKB approximation is able to capture the behavior of the magnitude modi cation due to the ltering e ect of critical levels. Hence, the validity of this method across z_c is ensured.

3.3 Results and comparison

With the two methods described in the last section, we are now ready to solve equation (3.3). The numerical results are assumed to be more accurate than the WKB method, and will serve as a reference for the comparison with the WKB approximation. In this section, calculation results of the following quantities for di erent wind pro les will be discussed and compared, namely the surface drag $\mathbf{D} = (D_x; D_y)$ and the wave momentum uxes $M = (M_x; M_y)$. The numerical integrations of these quantities are approximated by using the composite trapezoidal rule over the polar coordinate, with = 2 =1007.

Surface drag $\mathbf{D}$

Similar to the de nition of the surface drag in the 2-D case (2.21), the surface drag for ow over a 3-D isolated mountain is also de ned as the integral of the pressure gradient force over the orography. However, it becomes a vector instead of a scalar.

$$\mathbf{D} = \int_{-1}^{1}$$

Momentum uxes M

Using Parseval's theorem, the 3-D momentum uxes can be calculated as,

$$M_x = 4^2 \int_0^{\infty} \int_{-\infty}^{\infty} \hat{\tau}_{xw} \, dk_1 dk_2 \qquad \text{(3.46a)}$$

$$M_{44} \; ^2 4.637 \; _1 Td \; [\,(0)\,]TJ/F50 \; 10.9091 \; Tf \; 6.55 \; 16.47.78Td \; [\,(Z)\,]T$$

3.3.1 Linear wind pro le

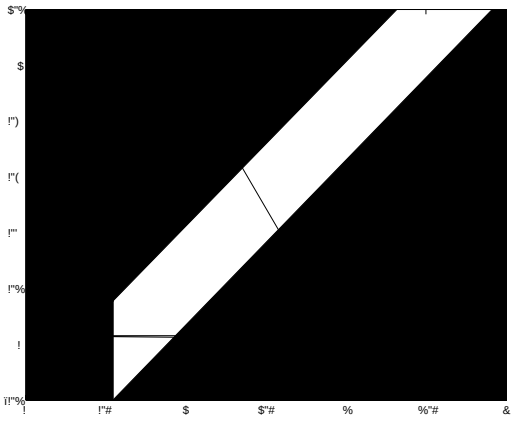

(a) x-momentum ux (Linear wind) : Ri = 1

(b) y-momentum ux (Linear wind): Ri = 1

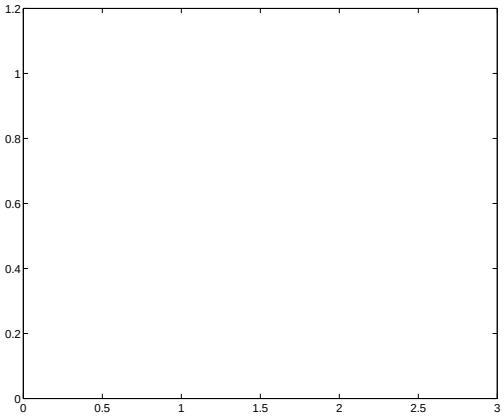

(c) x-momentum ux (Linear wind): Ri = 0:35

(d) y-momentum ux (Linear wind): Ri = 0:35

Figure 3.6: shows the x (left column) and y (right column) components of the momentum ux for the linear wind pro le with $Ri = 1$ on the rst row and $Ri = 0:35$ on the second row. The blue solid lines are WKB solutions, while the green dashed lines are numerical solutions. The WKB solution for w' is extended to 3rd-order in $''$ to achieve 2nd-order accuracy in the momentum uxes.

As shown in the above gures, the momentum uxes in the case of a linear wind pro le show a general decaying trend with z. This is de nitely due to the e ect of critical levels, at which a large portion of the wave energy of a certain wave number is attenuated and absorbed, hence causing a large drop of wave amplitude by a factor of e . As the wind direction turns with height, a greater and greater fraction of the wave numbers have been directionally ltered and hence the total momentum uxes drop signi cantly as z increases.

Both normalized ux components take values slightly lower than 1 at the surface. This is also explained by the fact that the wind shear acts to reduce the surface drag in the case of a linear wind pro le. Thus, the smaller Ri is, the smaller the momentum uxes at the surface, as shown clearly in gure (3.6(a)) and (3.6(c)).

For the linear wind pro le, the WKB method provides a accurate solution for the momentum ux, even when Ri^{-1} is not too small, e.g. $Ri^{-1} = 1$ in the rst row of gure (3.6). When $Ri = 0:35$, the surface drag computed with the numerical solution becomes lower than that computed with the WKB method. This is consistent with the di erence in surface drag variation

shown in gure (3.5).

For the momentum uxes, the overall distribution of the x-component is similar to that of the linear wind pro le, while the y-component is closed to 0 at the surface a4(at 0 G 0 g 0 G BT re99(tacs)-2helo

Chapter 4

Flow Over a 3-D Isolated Mountain in the Non-hydrostatic Regime

In the last chapter, an investigation was carried out in the hydrostatic framework, in which the magnitude of wave numbers forming the orography pro le were much smaller than the Scorer parameter $l(z)$. This condition is formally valid when the non-dimensional parameter $\hat{a}$ satis es $\hat{a} = \frac{Na}{|U_0|} \gg 1$, which means that the width of the mountain a is large and(or) the mean ow velocity $|U_0|$ is slow. The consequence is that the term k_{12}^2 can be dropped in (3.1) and waves can freely propagate in the atmosphere without being re ected. In this chapter, this condition will be relaxed by considering narrower mountains or faster mean winds. Hence the k_{12}^2 term is not negligible in (3.1). This creates regions where vertical wave propagation is prohibited and only evanescent waves exist, and at the same time wave re ection e ects have to be considered.

The associated di culty is that both the WKB approximation and the numerical method proposed by Siversten (1972) face technical problems in solving for $w(z)$. The WKB method fails in the vicinity of classical turning points, where propagating waves become evanescent, due to the fact that $l^2(z) - k_{12}^2$ becomes zero and changes its sign, and hence its magnitude cannot be regarded as slowly varying, which clearly con icts with the typical assumption of the WKB approximation. Solution to this problem up to rst-order is possible by using the so-called connection formulas, which involve the use of Airy functions (related with the modi ed Bessel function of order 1/3). However, due to the fact that extension of this method to higher orders must be required for the calculation of the momentum uxes with the required accuracy, this approach is not investigated in this study.

Again, the same two wind pro les will be studied, which are the linear and the turning wind pro le. In fact, an exact solution for the linear wind pro le in the case of a 2D mountain ridge had been studied by Wurtele et al. (1987), which can actually be easily extended to the situation of a linear wind pro le in ow over a 3D orography with directional shear. The derivation will be illustrated in detail in this chapter.

For the turning wind pro le, due to the phenomenon of wave re ection, the inclusion of a

second layer of atmosphere (e.g. the stratosphere), where the wind shear and curvature are assumed to be zero, will be important for the well-posedness of the problem. The detailed

Following the approach by Wurtele et al., rst, we restrict our attention on one side of the critical level. Without loss of generality, we consider $z > z_c$. Then, we transform the point of reference to the critical level by letting $= z \quad \frac{U_0(k_1+k_2)}{k_1} > 0$. Hence, above the z_c, equation (4.1) can be rewritten as

$$\frac{d^2w}{dz^2} + \left(\frac{\frac{N^2k_{12}^2}{(\ k_1)^2}}{\frac{U_0(k_1+k_2)}{k_1} \quad z}^2 \quad k_{12}^2 \right) w = 0$$

$$\frac{d^2w}{d\ ^2} + \left(\frac{Ri}{2} \quad k_{12}^2 \right) w = 0; \tag{4.3}$$

where $Ri = \frac{N^2k_{12}^2}{(\ k_1)^2}$ follows the same de nition as (A.5) in appendix A. Equation (4.3) in fact takes the same form as equation (2) in the paper by Wurtele et al. (1987), which has a general solution of the form

$$w(\ > 0) = C_1 \sqrt{\ } L_i\ (k_{12}\ ) + C_2 \sqrt{\ } K_i\ (k_{12}\ ); \tag{4.4}$$

where C_1, C_2 are constants to be determined, $= \sqrt{Ri \quad 0.25}$, and

that we only consider $z > z_c$. For

Re(m) = $^{0}(z)$ = 0 for $z > z_c$. In fact, Re(m) = $^{0}(z)$ means that the vertical momentum ux can be non-zero only when there is some phase variation of the complex argument of $\hat{w}(z)$ with respect to z, as shown by the real and imaginary parts of $\hat{w}$ in the region $z < z_c$ in gure (4.2(b)). Thus, xing a particular wave number k, above the corresponding critical level z_c, its contribution to the momentum ux is 0. This is, in fact, due to the re ection of waves in the upper atmosphere $z > z_c$, which kills o the term including of L_i and balances out the upward transport of horizontal momentum. In other words, this is the result of wave interference.

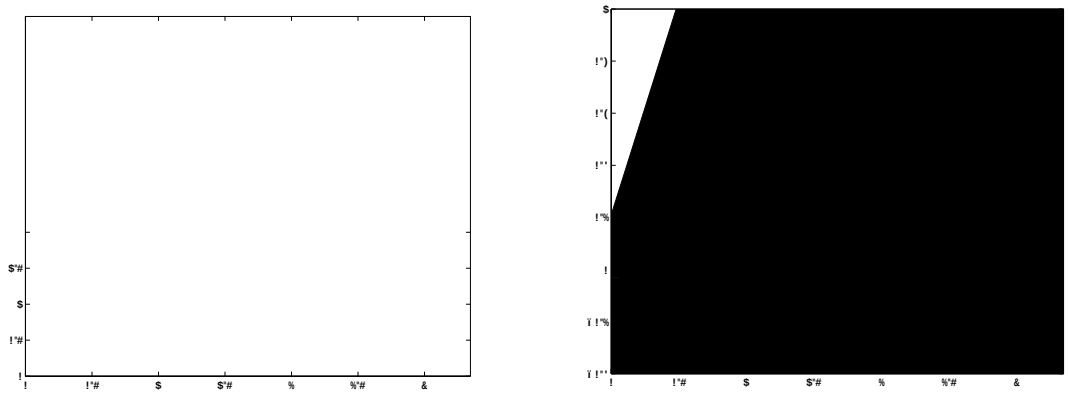

(a) Square of the Scorer parameter l^2

(b) Real and imaginary parts of $\hat{w}(z)$

Figure 4.2: (a) shows the distribution of the square of the Scorer parameter $l^2(z)$. The vertical black solid line indicates the critical level, the red horizontal line indicates the value of k_{12}^2. The two vertical dashed lines are the levels where transitions from the wave propagating regime to the evanescent regime occur (a broad wave propagating zone is located at the centre of the gure, while two narrow evanescent zones are located on the two sides of the gure). (b) shows the real (blue) and imaginary (green) parts of $\hat{w}(z($

ciated with this wave number is all re ected by the upper atmosphere due to non-hydrostatic e ects. In fact, this e ect has a large impact on the surface drag and the momentum uxes, as will be discussed in a later section.

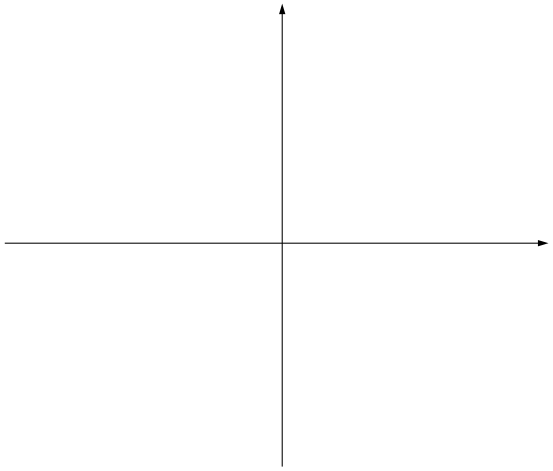

Figure 4.3: shows the plane of horizontal wave numbers k, which is divided into three di erent regions according to the height of the critical level. For the blue region, if a certain wave vector has its critical level located in this region, then the associated z_c must be within the calculation domain, as shown by the blue arrow (which indicates the wave number) and the blue dashed line (which indicates the wind direction perpendicular to the wave number). For the green region, if a certain wave number has its associated z_c in this region, then z_c must be above the calculation domain. Similarly, if some wave numbers have their perpendicular direction lying within the orange region, then their critical levels will be below the surface, as shown by the orange arrow and dashed line.

4.2.1 Results and discussion

Recall from chapter 3, that the surface drag and momentum ux had been expressed by (3.42)

enhancement in the x-component and a strong drag reduction in the y-component. Thirdly, both x and y components show strong drag reduction as the system becomes more non-hydrostatic. Fourthly, as the system becomes more non-hydrostatic, the surface drag varies with Ri^{-1}

Momentum uxes

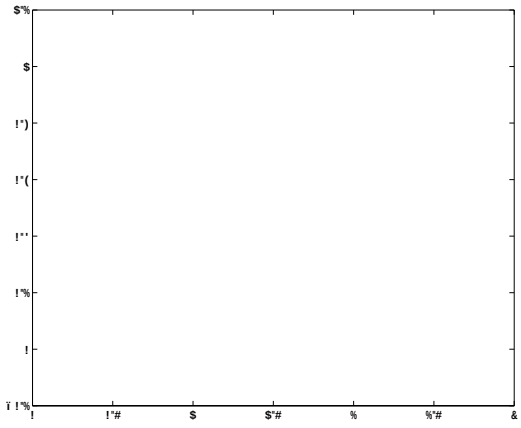

(a) $M_x = M_{x0}$; Ri = 1 with di erent ^ a

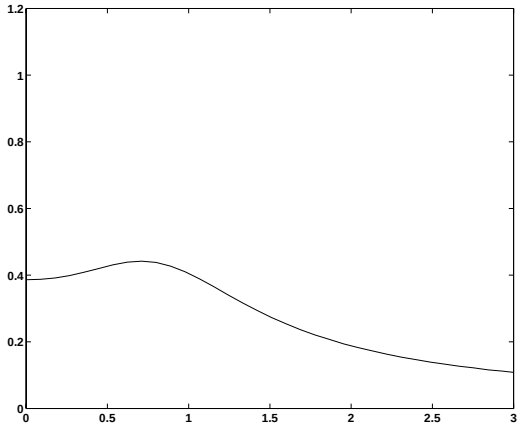

(b) $M_y = M_{y0}$; Ri = 1 with di erent ^ a

(c) $M_x = M$

dashed line, while the y-component shows a signi cant reduction when $a \gtrsim 4$ (which is actually still true for even larger a), and the reduction is further enhanced when a gets smaller. This

that, in the example illustrated, one critical level appears near the surface, while another critical level is about to appear at the top of the calculation domain. Therefore, to avoid the appearance of multiple critical levels, it is necessary to include another layer of atmosphere, in which the basic wind stops turning. The simplest choice is a pro le with constant wind. To guarantee continuity of the basic wind, the basic wind $U(z > H)$ in the second layer is set to be equal to the wind at the top of the rst layer ($z = H$), as shown in gure(4.6(b)). Additionally, for simplicity, it is assumed that the stability coe cient N is the same in both layers.

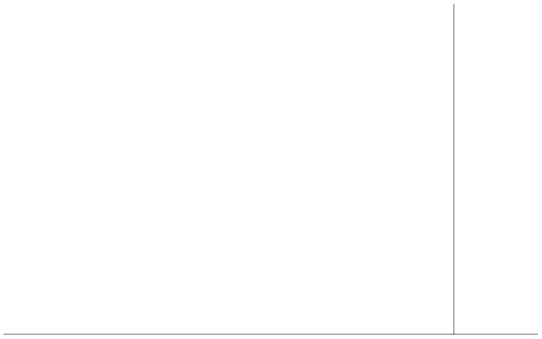

(a) square of the Scorer parameter $l^2(z)$ (b) 3D schematic diagram of wind pro le

Figure 4.6: (a) shows the periodic nature of the square of the Scorer parameter $l^2(z)$. The black vertical line on the left denotes the bottom of the domain, while the one on the right denotes the top of the domain. A critical level is located near the bottom of the domain (indicated by the vertical red dashed line), while another critical level is about to appear at the top of the domain (indicated by the vertical blue dashed line). (b) shows a 3D schematic diagram of the wind pro le in the two-layer atmosphere. In the second layer, the wind is constant and equals the wind at the top of the rst layer, so that continuity of the basic wind is guaranteed.

4.3.2 Numerical method

As mentioned above, in the non-hydrostatic limit, the vertical wave number of the waves m suffers from severe blow-up behaviors as the wave solution $\hat{w}$ changes from evanestent to vertically-propagating or vice-versa. Such blow-up behaviors makes the numerical method proposed by Siversten (1972) hard to implement. Therefore, an alternative numerical method must be used. Here, a numerical method will be proposed to solve the 3D Taylor-Goldstein equation (3.1) directly for $\hat{w}(z)$.

This is facilitated by the fact that if the basic wind turns by an angle of within the calculation domain, then any horizontal wave number k will have exactly one critical level within the domain. Then, with the aid of the asymptotic expressions for $\hat{w}$ and their derivatives near the critical level, as derived in appendix A, we are able to solve the Taylor-Goldstein equation as an initial-value problem, starting from the critical level.

Using the formula for the wind pro le (3.6), the non-hydrostatic steady-state Taylor-Goldstein

equation can be simpli ed as,

$$w''(z) + \frac{N^2}{\quad}$$

where C is some constant to be determined and m is de ned as

$$m$$

On solving, the three coe cients are

$$A = i\hbar U_0 k^{\frac{\hbar U}{}}$$

4.3.4 Results and discussion

Surface drag

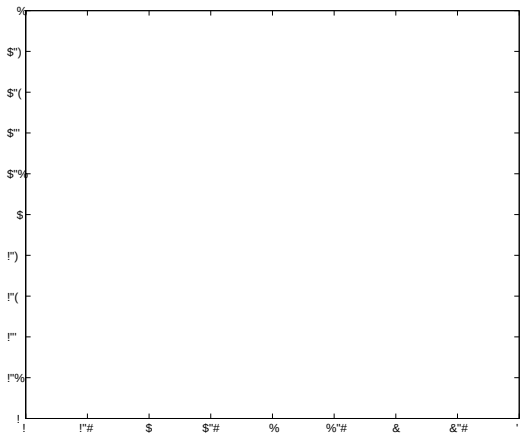

(a) Normalized x-component the surface drag

(b) Normalized y-component the surface drag

Figure 4.7: shows the two components of the normalized surface drag as a function of Ri^{-1}. All values are normalized by the surface drag in the hydrostatic limit, with $Ri = 1$. Figure (a) shows the distribution of the x-component for different values of α

Momentum uxes

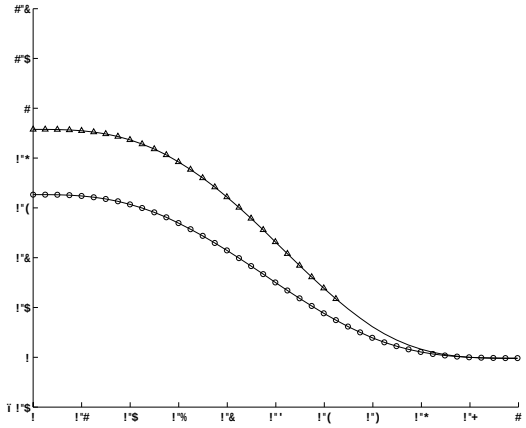

(a) M_x/M_{x0} for Ri = 1 with di erent ^ a

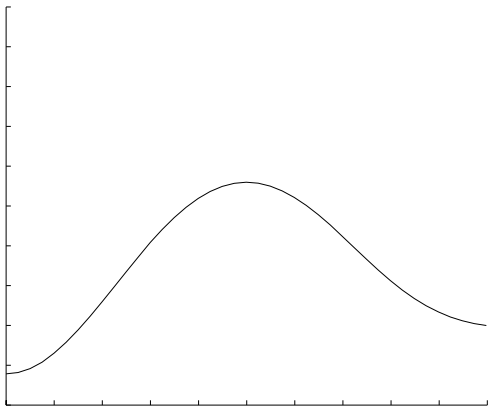

(b) M_y/M_{x0} for Ri = 1 with di erent ^ a

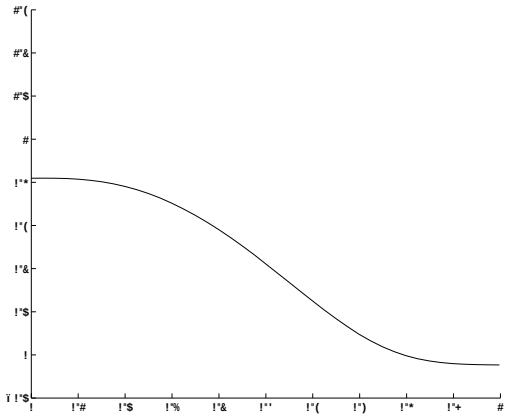

(c) M_x/M_{x0} for Ri = 0:5 with di erent ^a

(d) M_y/M_{x0} for Ri = 0:5 with di erent ^a

Figure 4.8: show the two components of the normalized momentum ux as a function of $z/$. All values are normalized by the surface drag in the hydrostatic limit, with $Ri = 1$. The left column ((a), (c)) shows the distribution of the x-component with for values of a, while the right column ((b), (d)) shows the y-component instead. The rst row has a Richardson number Ri =1, while the second row has $Ri = 0:5$. Symbols are used to denote di erent values of a,^i.e. circles indicate $a = 1:25$; triangles indicate $a = 2$; while diamonds indicate $a = 4$. The red dashed curve in each gure is the distribution of the momentum ux in the hydrostatic limit for the same values of Ri, which serves as a reference to assess non-hydrostatic e ects.

For the turning wind pro le, non-hydrostatic e ects have a large impact on the two components of the momentum ux pro les, showing a signi cant reduction of the surface drag as a increases. For the x-component, the changes are mainly in the momentum ux values near the surface, while the entire distribution retains its shape. The fractional decrease in magnitude is similar for the two values of Ri, being in both cases around 55%. Compared to the case of a linear wind pro le with directional shear, the slight surface drag enhancements that were observed when $a = 4$ are absent here for both Ri values.

However, for the y-component, besides the drop in the surface drag, non-hydrostatic effects lead to a significant modification in the distribution of the momentum flux. When $Ri = 1$, the y-component of the surface drag in the hydrostatic limit is about 0. So, the decrease of the drag due to non-hydrostatic effects (when $\hat{a}$ becomes small, e.g 2 or 1.25) leads to a negative y-component of the momentum flux near the surface. The y-momentum flux value then increases with z and reaches a positive maximum at around the middle of the calculation domain, as shown in figure (4.8(b)). However, when $Ri = 0.5$, since the y-component of the surface drag increases to a larger positive value in the hydrostatic limit, then the decrease of the drag value due to non-hydrostatic effects cannot bring its value down to below 0. So, the overall y-component of the momentum flux remains positive throughout the atmosphere.

Moreover, compared to the corresponding result for the linear wind profile, the y-component of the momentum flux does not show a significant drop by a factor of about $1/\sqrt{2}$. This is because the turning wind profile turns by an angle of within the first layer of the atmosphere, so any wave number k has one critical level within the domain, which protects the upward-propagating waves from the interference due to downward propagating waves. Hence, if $\hat{a}$ is large, e.g. $\hat{a} \geq 4$, then the momentum flux profile tends to the hydrostatic limit, indicated by the red dashed curves in figures (4.8(b)) and (4.8(d)). This also corroborates that the significant reduction in the y-component of the momentum flux in the case of the linear wind profile is due to the critical-level-free zone in the wave number plane, i.e. the orange region in figure (4.3), in which all of the y-component momentum flux is reflected back to the surface by downward propagating waves.

Chapter 5

Concluding remarks and future work

This dissertation explored the behaviors of two important quantities, namely the momentum flux and surface drag associated with mountain waves generated by an isolated mountain, in both the hydrostatic and non-hydrostatic regimes. In this chapter, the main findings will be summarized in separate sections, and then followed by a description of possible future works.

5.1 Analysis of methods

Various approaches have been investigated and successfully applied. Assuming non-rotating, linearized flow with the Boussinesq approximation, the exact solution to the mountain wave problem for a linear wind profile with directional shear in the non-hydrostatic limit has been successfully derived, which in theory is also valid in the hydrostatic regime by assuming that the magnitude of the horizontal wave vector k_{12} is small. The exact solution is based on the fundamental work by McFarlane (1987). The WKB approximation, which is only valid in hydrostatic limit, has been examined following the approach by Teixeira and Miranda (2004), and similar results were successfully reproduced. The numerical method developed by Siversten (1972) was also successfully manipulated and the results showed excellent agreement with the WKB approximation in the case of a linear wind profile. With the aid of the exact solution for the linear wind profile, the accuracy of the numerical method has been demonstrated, and hence this method could be safely applied to the turning wind profile case. In the non-hydrostatic

5.2 Calculation results

5.2.1 Hydrostatic regime

In the hydrostatic limit, variations of the surface drag as a function of Ri^{-1} for the two wind profiles exhibit different behaviors. For the linear wind profile, both components of the surface drag keep decreasing throughout the range of Ri^{-1} from 0 to 4; while for the turning wind profile the surface drag shows an increasing trend as Ri^{-1} increases. This difference is in fact

For the turning wind pro le, a second layer of atmosphere is added on top of the original calculation domain, which has constant static stability, density and basic wind. The basic wind velocity in this additional layer takes the same value as at the top of the rst layer so that continuity of the wind pro le is guaranteed. Due to the periodicity of occurrence of critical levels with height in the turning wind pro le, the second layer avoids the complications arising from the e ects of multiple critical levels and wave re ections. In this atmospheric con guration, the increasing trend of the surface drag as a function of Ri^{-1} which was observed in the hydrostatic regime is suppressed when Ri^{-1} gets close to 4. This is caused by the stronger wave re ection e ect that occurs when Ri is small. This is also the reason why the variation of the surface drag becomes more non-linear as the system becomes more non-hydrostatic. Concerning the momentum uxes, both components of this quantity show a large drop in magnitude near the surface when the system becomes more non-hydrostatic. Besides this change, when Ri is large, the y-component of the momentum ux near the surface takes negative values but changes its sign to positive as z increases.

5.3 Overall e ect of non-hydrostaticity

From the changes found in the investigation of the non-hydrostatic mountain wave system, the general e ect of non-hydrostaticity is that of causing a signi cant reduction to both the surface drag and the momentum uxes near the surface. Such a reduction is crucial, since current drag parametrization schemes are mainly based on the hydrostatic assumption, which may thus overestimate the momentum and energy transport by terrain-generated gravity waves.

All the derivations and calculations carried out here assumed a non-rotating, inviscid, adiabatic, linearized ow with the Boussinesq approximation. Diabatic and non-linear e ects have all been neglected for simplicity, since these e ects may cause unnecessary complications in the adopted conceptual model.

5.4 Future work

In the investigation carried out in this dissertation, there are three main lines of further work that can be pursued. Firstly, the atmospheric setting for the linear wind pro le in non-hydrostatic conditions is in fact unrealistic due to the fact that in reality the basic wind magnitude cannot keep increasing with z inde nitely. Typically, as the stratosphere is reached, the atmosphere becomes much more stable and hence more favourable for wave propagation. Hence, a two layer model for such a linear wind pro le in non-hydrostatic conditions is worth being considered to obtainis more28(tum)on 8f 8J -133.9
non-hydrostaticity. signi ca19 ownsns-1698(rlaitiv)27(e)-468(oe)-468(hue)-693ppreeanttsbehbhalt
the prnmoucred
nt, occu,Hence,the currnsponding s(v)28(ehe)-288(reduction)-278(of)-398(the)2978(surface)-978(drag)-285(

Secondly, the maximum turning angle of the turning wind pro le may also play an important role in modifying the variation of the surface drag and momentum uxes. When the basic wind turns by an angle of , all wave numbers have exactly one critical level within the domain. However, this is clearly not always true for the real atmosphere. If the turning angle is less than , then some wave numbers will not have a critical level within the atmosphere, and hence wave re ection may strongly a ect those wave numbers. Therefore, the dependence of the drag and momentum uxes on the turning angle would be an interesting problem for investigation.

Thirdly, non-hydrostaticity can also be studied more thoroughly. Since a non-hydrostatic system is $\hat{a}$-dependent, quantities like the surface drag become dependent on both R_i and $\hat{a}$. Hence, accurate parametrization schemes for surface drag must capture that dependence as well, which justi es investigating it in more detail.

Bibliography

Lott, F. and M. J. Miller, 1997: A new subgrid-scale orographic drag parametrization: Its formulation and testing. Quarterly Journal of the Royal Meteorological Society 123 (537), 101{127.

McFarlane, N. A., 1987: The e ect of orographically excited gravity wave drag on the general circulation of the lower stratosphere and troposphere.Journal of the atmospheric sciences, 44 (14), 1775{1800.

Miranda, P. M. A. and I. N. James, 1992: Non-linear three-dimensional e ects on gravity-wave drag: Splitting ow and breaking waves. Quarterly Journal of the Royal Meteorological Society, 118 (508), 1057{1081.

Nappo, C. J., 2012: An introduction to atmospheric gravity waves, Vol. 102. Access Online via Elsevier.

Satyanaryanan, A. and P. L. Sachdev, 1980: Re ection of internal gravity waves in an atmosphere with wind shear: Wkb approximation. Indian Journal of Pure and Applied Mathematics, 11 (12), 1696{1703.

Shutts, G., 1995: Gravity-wave drag parametrization over complex terrain: The e ect of critical-level absorption in directional wind-shear. Quarterly Journal of the Royal Meteorological Society, 121 (525), 1005{1021.

Shutts, G. J., 1998: Stationary gravity-wave structure in ows with directional wind shear. Quarterly Journal of the Royal Meteorological Society 124 (549), 1421{1442.

Shutts, G. J. and A. Gadian, 1999: Numerical simulations of orographic gravity waves in ows which back with height. Quarterly Journal of the Royal Meteorological Society 125 (559), 2743{2765.

Teixeira, M. A. C. and P. M. A. Miranda, 2004: The e ect of wind shear and curvature on the gravity wave drag produced by a ridge. Journal of the atmospheric sciences, 61 (21), 2638{2643.

Teixeira, M. A. C. and P. M. A. Miranda, 2006: A linear model of gravity wave drag for hydrostatic sheared ow over elliptical mountains. Quarterly Journal of the Royal Meteorological Society, 132 (620), 2439{2458.

Teixeira, M. A. C. and P. M. A. Miranda, 2009: On the momentum uxes associated with mountain waves in directionally sheared ows.Society

Appendix A

Behavior of gravity waves near a critical level

In this section, we will examine the behavior of gravity waves near a critical level by using the approach of Frobenius expansion. This analysis follows the treatment presented in the book by Nappo (2012) and we extend the idea a bit further to the case of a three-dimensional isolated mountain.

In the Taylor-Goldstein equation (A.1), the critical level is defined to be the height z_c at which the denominator, $U\ k = U(z)k_1 + V(z)k_2$, is zero. This means that at the critical level, the unperturbed wind $U(z)$ is perpendicular to the horizontal wave vector k. This produces a singularity (a second-order pole) in the Scorer parameter in equation (A.1), and hence the first-order derivative of $\hat{w}(z)$ is not continuous at the height z_c. Moreover, note that the square of the Scorer parameter l^2 is proportional to the square of the vertical wave number m of the gravity waves. As z approaches z_c, the Scorer parameter blows up to infinity. This implies that the gravity waves becomes highly oscillatory, as will be shown in the following discussion.

$$\frac{d^2\hat{w}}{dz^2} + \left(l(z)^2 - k_{12}^2\right)\hat{w} = 0 \tag{A.1}$$

where $l(z)^2$ is the square of the Scorer parameter, defined to be

$$l(z)^2 = \frac{N^2}{(U\ k)^2} + \frac{U''\ k}{U\ k} \tag{A.2}$$

Assume that we approach the critical level from above: then near the critical level, we write $z = z_c + \ $, where $\ $ is assumed to be a small positive distance from the critical level z_c. For convenience, define $G(z) := U(z)\ k$. We expand the function $G(z)$ near z_c by Taylor expansion

$$G(z_c + \ ) = 0 + G'(z_c)\ + \frac{1}{2}G''(z_c)\ ^2 + O(\ ^3) \tag{A.3}$$

Then, the square-root of the denominator in equation(A.2) can be approximated as

$$\frac{1}{G(z_c + \quad)} \quad \frac{1}{G^0(z_c) \quad + \frac{1}{2}G^{00}(z_c) \quad ^2}$$
$$= \frac{1}{G^0(z_c) \quad (1 + \frac{G^{00}(z_c)}{2G^0(z_c)} \quad)}$$
$$\frac{1 \quad \frac{G^{00}(z_c)}{2G^0(z_c)}}{G^0(z_c)} \tag{A.4}$$

Since we only consider simple linear and turning wind pro les, and the curvature term $G^{00}(z)=G(z)$ is constant in both cases, we use ^{2} to denote this term. Thus, the square of the vertical wavenumber (or $l^2 \quad k_{12}^2$) of the waves becomes

$$\frac{N^2 k_{12}^2 \quad 1 \quad \frac{G^{00}(z_c)}{2G^0(z_c)} \quad ^2}{^2(G^0(z_c))^2} + \quad ^2 \quad k_{12}^2$$
$$= \frac{N^2 k_{12}^2}{(G^0(z_c))^2} \quad \frac{1}{2} + \quad \frac{G^{00}(z_c)}{2G^0(z_c)} \quad ^2 \quad \frac{G^{00}(z_c)}{G^0(z_c)} \frac{1}{-} \quad ! \quad + \quad ^2 \quad k_{12}^2$$
$$= \frac{Ri}{2} \quad - + \tag{A.5}$$

where $Ri = \frac{N^2 k_{12}^2}{(G^0(z_c))^2}$ actually has the same scale as the Richardson number Ri, $= Ri \quad \frac{G^{00}(z_c)}{G^0(z_c)}$ and $= Ri \quad \frac{G^{00}(z_c)^2}{4G^0(z_c)^2} \quad + \quad ^2 \quad k_{12}^2$.

Rewriting equation(A.1), we have

$$\frac{d^2 w}{dz^2} + \quad " \quad \frac{Ri}{2} \quad - + \quad \# \quad w = 0: \tag{A.6}$$

The asymptotic behavior of $w(z)$ near the critical level z_c can be solved using a Frobenius expansion, by assuming $w(z_c +$

Thus, we require all the coe cients to be zero, and this yields the following relations

$$C_1 = \frac{}{(\quad + 1) + \quad Ri} \quad C_0; \tag{A.9}$$

$$C_2 = \frac{^2[\quad (\quad + 1)] \quad ^1}{(\quad + 1)(\quad + 2) + \quad Ri} \quad C_0 \tag{A.10}$$

and importantly

$$^2 \quad + \quad Ri = 0 \tag{A.11}$$

Actually, for both the two considered wind pro les, is 0, since the linear wind pro le has no curvature, and the simple turning wind pro le has $w^{00}(z_c) = \quad ^2w(z_c) = 0$, so some further simpli cations can be achieved, but this will not be presented here.

Equation (A.11) gives,

$$= \frac{1}{2} \quad i \tag{A.12}$$

where $= \quad \sqrt{Ri \quad 0{:}25}$. These two branches of correspond to the two members of the solution basis, and the general solution near z_c

and rewrite equation (A.13), just by replacing with , that is

$$\hat{w}(z_c\ \ ) = C_0^+(\ \ )^{+} A(\ \ ) + C_0(\ \ )\ \ A(\ \ ) \qquad \text{(A.14)}$$

However, a tricky point comes from the terms ( ) . This is because Re( ) = ^{1}

Thus, for $G^0(z_c) > 0$

$$\begin{aligned} (\quad) &= e^{\quad i} \\ &= e^{\quad i\frac{}{2}}e \\ &= \quad ie \end{aligned} \tag{A.18}$$

Similarly, for $G^0(z_c) < 0$, we have $\left(\quad i\frac{c_i}{G^0(z_c)}\right) \; ! \; e^i \;$ as $c_i \; ! \; 0$

$$\begin{aligned} (\quad) &= e^i \\ &= e^{i\frac{}{2}}e \\ &= ie \end{aligned} \tag{A.19}$$

In general, by letting $sgn = \text{sign}(G^0(z_c$

coe cient A if $sgn > 0$, thus it is associated with upward propagating energy. Similarly, it can be proved that if $sgn < 0$, the term with coe cient B is associated with upward propagating energy. Therefore, we see that the terms with e multiplied for $z < z_c$ always have upward propagating energy. The proof follows the same reasoning for waves with downward propagating energy.

This is a signi cant result, since it means that the critical level always lters the wave by multiplying it with a factor of e

Appendix B

Definition of Fourier integrals and the Parseval Theorem

The following definition of Fourier transform of an integrable function $f(x)$ in $(-1; 1)$ is adopted in the discussions of all the chapters,

$$\hat{f}(k) = \frac{1}{2} \int_{-1}^{1} f(x) e^{-ikx} dx \quad \text{and} \tag{B.1a}$$

$$f(x) = \int_{-1}^{1} \hat{f}(k) e^{ikx} dk; \tag{B.1b}$$

where $\hat{f}(k)$ is the Fourier transform of $f(x)$ and k is the wave number. With the above definition of Fourier integrals, the Parseval theorem

where the last equality uses the de nition of the Dirac delta function. Then,

$$\frac{1}{2}\int_{-1}^{1} f(x)g^{*}(x)dx = \int_{-1}^{1} \hat{f}(k_1) \int_{-1}^{1} \hat{g}^{*}(k_2)\,(k_1 - k_2)dk_2\,dk_1$$